Combined Electromechanical Impedance and Fiber Optic Diagnosis of Aerospace Structures

Jon Schlavin[a], Andrei Zagrai[a], Rebecca Clemens[a], Richard J. Black[b], Joey Costa[b], Behzad Moslehi[b], Ronak Patel[b], Vahid Sotoudeh[b], and Fereydoun Faridian[b]

[a]Department of Mechanical Engineering, New Mexico Institute of Mining and Technology, 801 Leroy Pl., 124 Weir Hall, Socorro, NM 87801 USA, azagrai@nmt.edu;
[b]Intelligent Fiber Optic Systems Corporation, IFOS, 2363 Calle del Mundo, Santa Clara CA 95054-1008 USA

ABSTRACT

Electromechanical impedance is a popular diagnostic method for assessing structural conditions at high frequencies. It has been utilized, and shown utility, in aeronautic, space, naval, civil, mechanical, and other types of structures. By contrast, fiber optic sensing found its niche in static strain measurement and low frequency structural dynamic testing. Low frequency limitations of the fiber optic sensing are mainly governed by its hardware elements, and as hardware improves, so does the bandwidth (frequency range * number of sensors). In this contribution we demonstrate simultaneous high frequency measurements using fiber optic and electromechanical impedance structural health monitoring technologies.

A laboratory specimen imitating an aircraft wing structure, incorporating surfaces with adjustable boundary conditions, was instrumented with piezoelectric and fiber optic sensors. Experiments were conducted at different structural boundary conditions associated with deterioration of structural health. High frequency dynamic responses were collected at multiple locations on a laboratory wing specimen and conclusions were drawn about correspondence between structural damage and dynamic signatures as well as correlation between electromechanical impedance and fiber optic sensors spectra. Theoretical investigation of the effect of boundary conditions on electromechanical impedance spectra is presented and connection to low frequency structural dynamics is suggested. It is envisioned that acquisition of high frequency structural dynamic responses with multiple fiber optic sensors may open new diagnostic capabilities for fiber optic sensing technologies.

Keywords: aircraft structural dynamics, electromechanical impedance, aircraft non-destructive evaluation, high frequencies, strain measurements, fiber optic sensors, FBG

1. INTRODUCTION

Structural Health Monitoring (SHM) is a growing technology that seeks to reduce the cost, time, and uncertainty of structural inspections. By utilizing embedded sensors, SHM continuously monitors a structure to detect early signs of damage thereby reducing maintenance costs and permitting replacement of deteriorated components on as needed basis. Historically, piezoelectric transducers have been the most common embedded sensors for SHM.[1,2] These transducers have been explored in variety of SHM methodologies ranging from active embedded ultrasonics,[3,4] to passive acoustic emission monitoring.[5] Among many other types of SHM sensors, optical fiber sensors drew particular attention because of multiplexability (many sensors on one fiber) and electromagnetic immunity. Such sensors primarily support passive strain measurements.[6] Their use in active damage detection was limited to a few cases where the fiber optic sensor was utilized to receive ultrasonic pulses transmitted by piezoelectric sensors.[3,6] This paper extends the approach of a combined fiber optic / piezoelectric system to high frequency structural dynamic measurements and demonstrates the use of fiber-Bragg grating (FBG) sensors in the electromechanical impedance SHM method. As a result, the system is advantageously broadband, spanning from static strain and temperature measurements to high frequency (hundreds of kHz) dynamic testing.

FBGs were first developed in 1978 making them a relatively new sensor technology.[7] They are one of the most common optical fiber sensors because they are relatively easy to manufacture.[8] FBG operation principle relies on fiber optic cables and wavelength shifting. Light is guided along a fiber optic cable due to the refractive

indices of the fiber keeping the light internally reflected. The cable can be turned into a sensor array by including Bragg gratings along the fiber. These gratings are periodic changes of the index of refraction of the fiber core along the longitudinal direction.[8] If the wavelength satisfies the Bragg condition (Equation 1) then the reflected light adds constructively while light of other wavelengths will pass through.

$$\lambda_B = 2n_{eff}\Lambda \tag{1}$$

Where λ_B is the Bragg wavelength, n_{eff} is the effective refractive index of the fiber, and Λ is the periodicity of the grating.[8] When the sensor is strained these patterns are stretched or compressed, changing Λ and shifting λ_B. This principle is illustrated in Figure 1. Multiple sensors can be placed on the same fiber by using different initial Λ values that are spaced out appropriately. Additionally these sensors are not affected by outside electromagnetic interference, which can degrade signals from other sensor types.

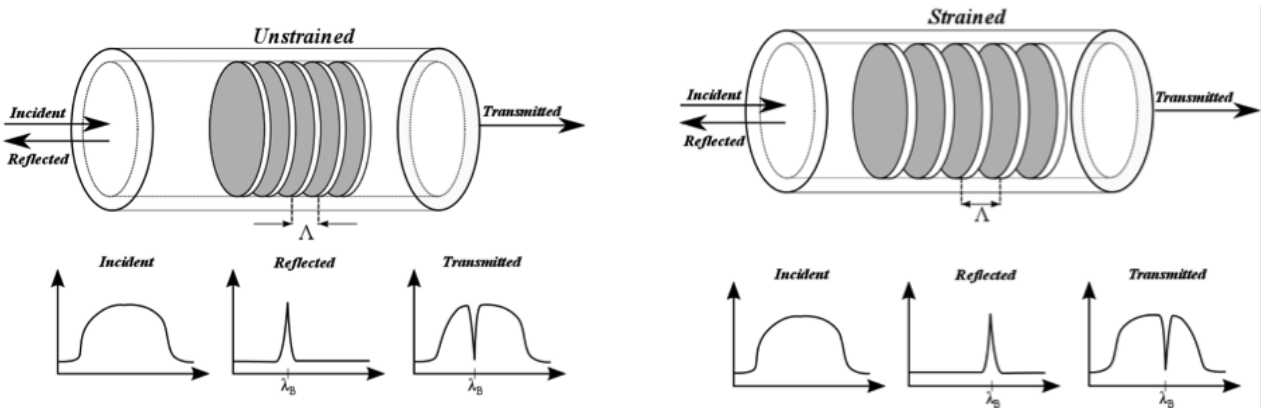

Figure 1. FBG functioning principle

Electro-mechanical Impedance (EMI) is a SHM approach that relies on high frequency continuous wave (CW) interrogation of piezoelectric transducers.[2] Due to the piezoelectric effect, transducers mechanical properties are manifested in its electrical impedance. When the transducer is bonded to a structure, the mechanical properties of the transducer are coupled with those of the structure via the adhesive bond. Therefore, damage-induced mechanical changes to the structure result in corresponding variations in the electrical impedance.[2,9,10] Original development of the electro-mechanical impedance method is due to Liang and colleagues.[11] For more than two decades, many other authors contributed to this method including, but not limited to, Chaudhry et al.,[12] Giurgiutiu and Rogers,[13] Park, et al.,[14] Zagrai and Giurgiutiu,[15] Tseng and Naidu,[16] Bhalla and Soh.[17]

The principle of the method can be described with the following equation including sensor and structural dynamics. Damage modifies structural dynamic properties and therefore is reflected in the cumulative (sensor and structure) electro-mechanical impedance measured at the piezoelectric sensor terminals.

$$Y(\omega) = \frac{I(\omega)}{V(\omega)} = i\omega C\left(1 - \kappa_{31}^2\left(1 - \frac{1}{\varphi cot\varphi + r(\omega)}\right)\right), r(\omega) = \frac{k_{str}(\omega)}{\kappa_{PWAS}^b} \tag{2}$$

where C denotes the zero-load capacitance and κ_{31} represents the coupling coefficient of piezoelectric active sensor for in-plane vibration, k_{str} and k_{PWAS} are structural and sensor stiffnesses respectively, and admittance $Y(\omega)$ is the inverse of impedance and is dependent on the interrogation frequency. Typically, EMI method sweeps through frequency ranges and saves impedance data for all frequencies to develop a frequency response reflecting structural dynamic behavior.

2. ELECTRO-MECHANICAL IMPEDANCE MEASUREMENT EQUIPMENT

Many devices exist to measure impedance data from piezoelectric transducers including the Hewlett Packard 4192A Impedance Analyzer, Cypher Instruments C-60 Impedance Analyzer, and Wireless Impedance Device

(WID3) microcontrollers developed at Los Alamos National Lab (LANL).[18] Each of these systems are shown in Figure 2 in the progression that shows size (and mass) reduction over time.

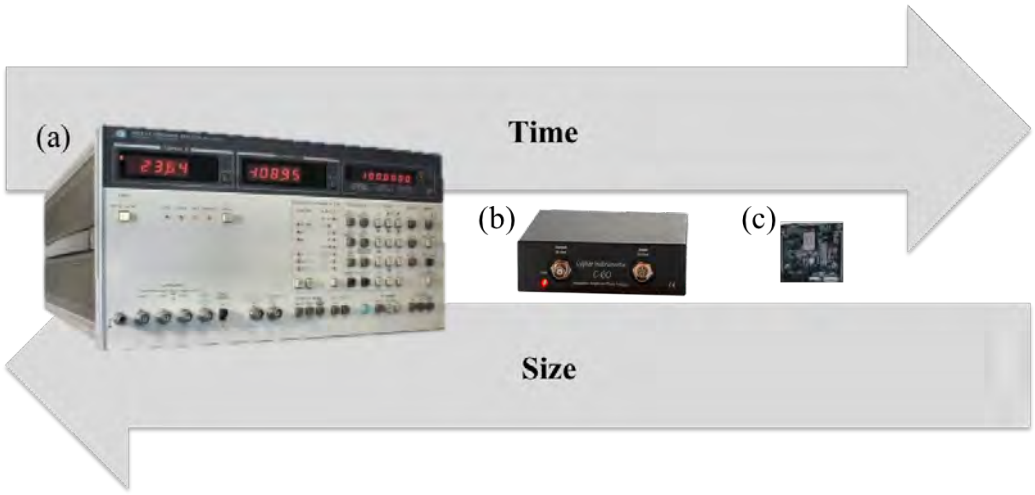

Figure 2. Impedance Analyzers: (a) HP 4192A, (b) Cypher Instruments C-60, (c) LANL WID3

The HP analyzer has been used extensively in research of EMI but is large and requires special programs (like LabView) to control and store data. The C-60, a portable version of impedance analyzer, has not been used as widely but is very light and comes with software to control it. The WID3, and similar other boards developed by researcher around the world, is much smaller but is less reliable and must be programed in special language to operate. Because of a need for portable equipment in field impedance measurement, our group considered the C-60 unit. In order to investigate impedance representation in C-60, experiments were performed to compare the newer, more portable analyzer to the HP4192A. The tests included testing piezoelectric transducers in free-free boundary conditions and while bonded to a structure. Comparison of HP4192A vs. C-60 is given in Figure 3.

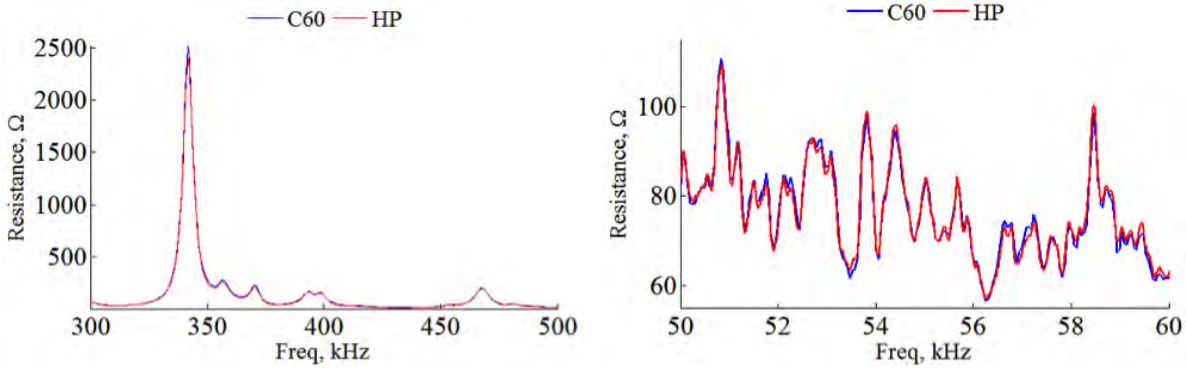

(a) piezoelectric transducer only (b) piezoelectric transducer bonded to a structure

Figure 3. Comparison of HP and C-60 Impedance Analyzers

Based on these tests it was determined that the C-60 rather accurately represents both sensor and structural impedances. Benefits of C-60 included increased portability and ease of operation. The main limitation was a reduced number of data points as the C-60 had a limit of 1024 data points per test.

3. DETECTING LOOSE BOLTS USING ELECTRO-MECHANICAL IMPEDANCE METHOD

Detection of loose bolts is a common application of the EMI method.[2,9] In this study EMI method was used to detect loose bolts on a simple aerospace structure and different measures for determining if damage had occurred were considered and compared.

3.1 Experimental setup and procedure

The experiments were conducted on a representative wing structure depicted in Figure 4. The structure was composed of 6061 aluminum sheet constructed into a rough wing-shaped with two adjustable stiffness flaps on the trailing edge. Two aluminum L-beams were bolted together with the wing in the middle to imitate a structural joint. The wing was instrumented with five piezoelectric transducers, five fiber-Bragg grating strain sensors, two accelerometers, and a PCB strain gauge as illustrated in Figure 4(a).

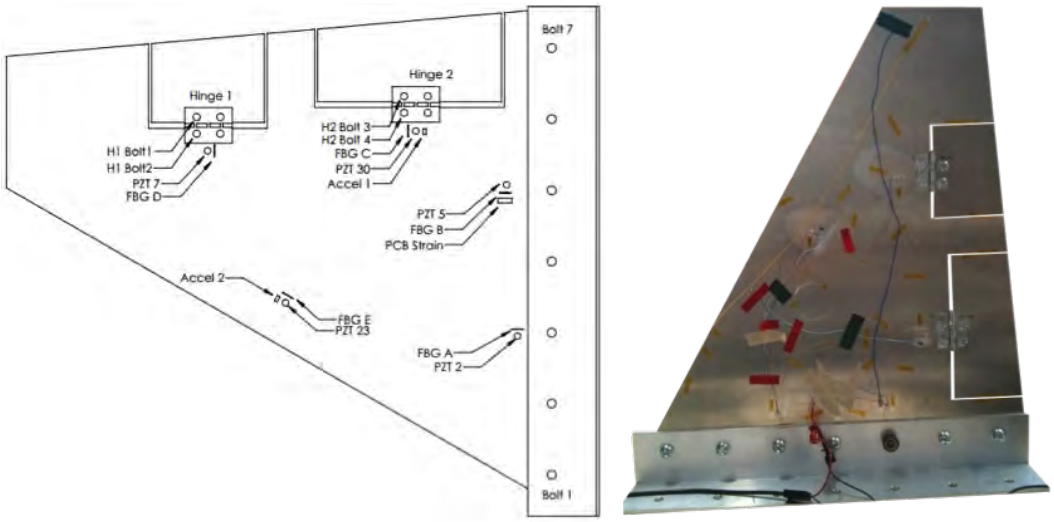

(a) schematic of structure with sensor locations (b) photograph of specimen

Figure 4. Wing Structure used in experiments

The condition of the bolted joint was adjusted using an LCWD-5k Load Washer mounted on a 40mm M10 flange bolt according to the schematic given in Figure 5. The force transmitted through the bolt was measured by connecting LCWD-5k to a power supply and PXIe-1062Q digitizer; LabVIEW was utilized to process and visualize the data. When testing the wing structure, the impedance analyzer was set to run from 50-100kHz. This range was selected due to high density of peaks in structural response. Two types of measurements were conducted: impedance analysis measurements only and simultaneous impedance analysis and fiber optic system data acquisition. In the first case, 1024 data points were collected resulting in a frequency step of 48Hz. In the second case, due to time parameters of the FBG data acquisition system, 168 data points were collected yielding a frequency step of 300 Hz. The fiber-optic system measured strain data from all five FBG sensors in the time domain with a synchronous sampling rate of 500 kHz.

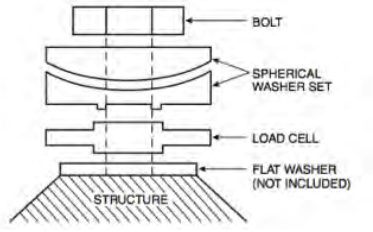

Figure 5. Load Cell installation scheme

3.2 Damage Metrics

Multiple metrics have been proposed in the past for determining if a bolted joint is damaged based off EMI data including root mean square deviation (RMSD) and correlation coefficient deviation (CCD),[19] equations for which are given in (3) and (4), respectively.

$$RMSD = \sqrt{\sum_{n} \frac{\left(Re(Z_i) - Re(Z_i^0)\right)^2}{\sum_n [Re(Z_i^0)]^2}} \tag{3}$$

$$CCD = 1 - \left[\frac{1}{\sigma_Z \sigma_{Z^0}} \sum_{n} [Re(Z_i) - Re(\bar{Z})] \times [Re(Z_i^0) - Re(\bar{Z}^0)] \right] \tag{4}$$

Additionally the energy of the structure can be found by finding the area under the curve of the real part of the impedance. By breaking this curve into bins you can determine what frequency range has how much energy. For this study this method was referred to as the energy method. An additional method that has been proposed is fitting a high (7-9th) order polynomial to the real part of the impedance data. This essentially is a low-pass filter from which you can see the general trends of the data.

3.3 Analysis of joint integrity

Experiments were conducted using the load sensor to quantify the integrity of the bolted joint while piezoelectric transducers measured the response of the structure from 50-100 kHz. In the specimen depicted in Figure 4, bolt 5 has been monitored with PZT 5. Using the load sensor, different loads were applied to the bolt at discrete loads: $13,344N(3000lb_f)$, finger tight $222N(50lb_f)$, $890N(200lb_f)$, $2224N(500lb_f)$, $4448M(1000lb_f)$, $6672N(1500lb_f)$, and $8896N(2000lb_f)$. Structural responses generated from this experiment are seen in Figure 6.

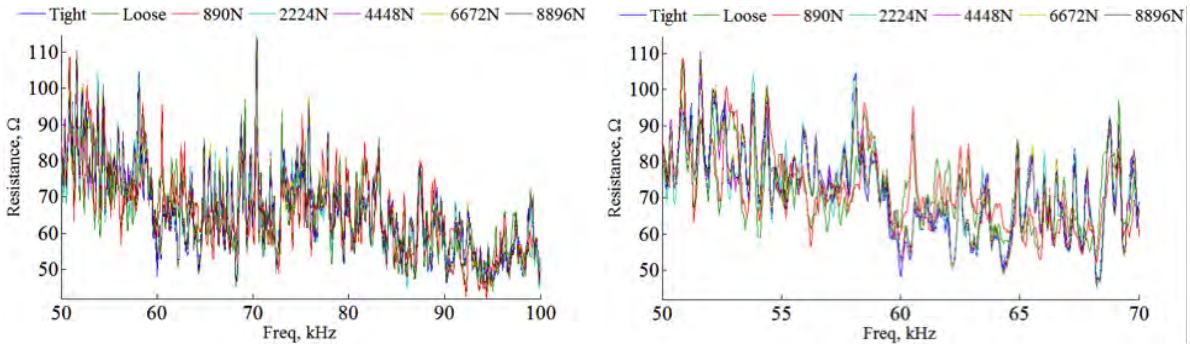

(a) Complete frequency range (b) Closer look at a portion of response

Figure 6. Structural response from bolted joint

Damage detection metrics described by equations (3) and (4) were applied to the data in bolted joint experiment and results are presented in Figure 7 . In the figures, test 1 signifies the bolt tightened to 13,344 N, and tests 2-7 indicate conditions ranging from loose to tighter in the increments given above. As can be seen in Figure 7(a) and (b), RMSD and CCD for test 1 are zero, metrics increase for the first two cases of relatively loose bolt and then reduce for tight conditions. Figure 7(a) and (b) suggest two important conclusions: (1) in the presented setup, integrity of bolted joint is presented as a binary scenario loose, first two cases, and tight, last four cases; (2) CCD indicates larger difference between loose and tight cases, which could be beneficially used in damage detection algorithms.

Figure 7(c) illustrates electro-mechanical impedance spectra and its energy representation acquired under different conditions of the joint. Due to different loads, some peaks in the impedance response are shifted and amplitude is changed in certain frequency bands. The lower portion of the figure was obtained for the real part of impedance by calculating area under the curve within 5 Hz segments. Interestingly, green and red bars corresponding to finger tight and low load conditions often show behavior distinct from other bars, such as in frequency bins 2, 3, 5, and 9. Some frequency bins, however, show these bars behaving comparable to other bars, e.g. 10 and 6. This observation highlights necessity for considering different frequency bands while analyzing the electro-mechanical impedance data. In general, results obtained from energy plot correlated with results provided by statistical metrics such as RMSD and CCD.

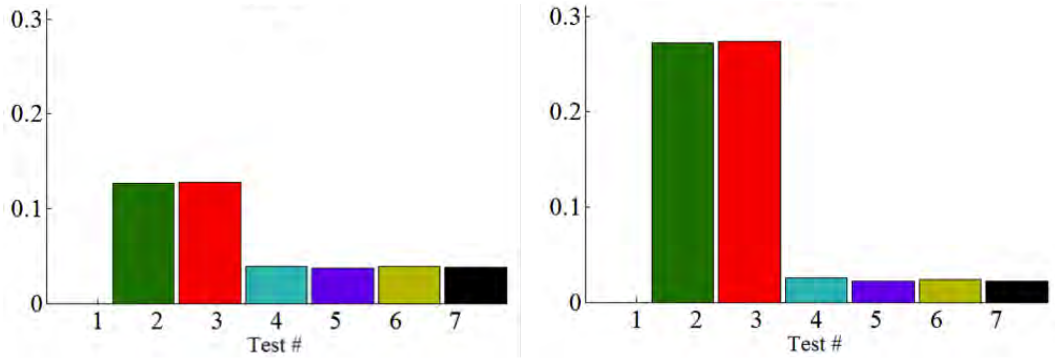

(a) RMSD

(b) CCD

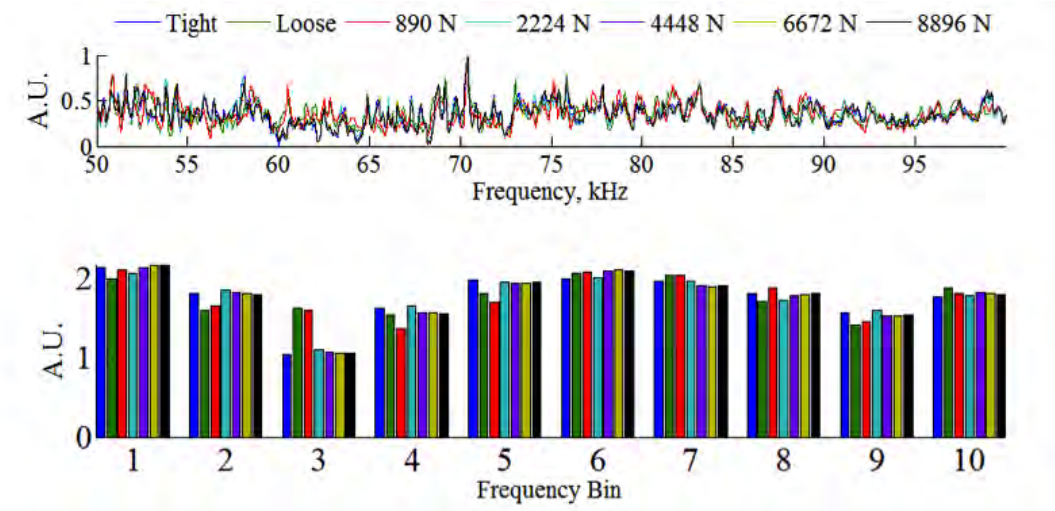

(c) Energy Method

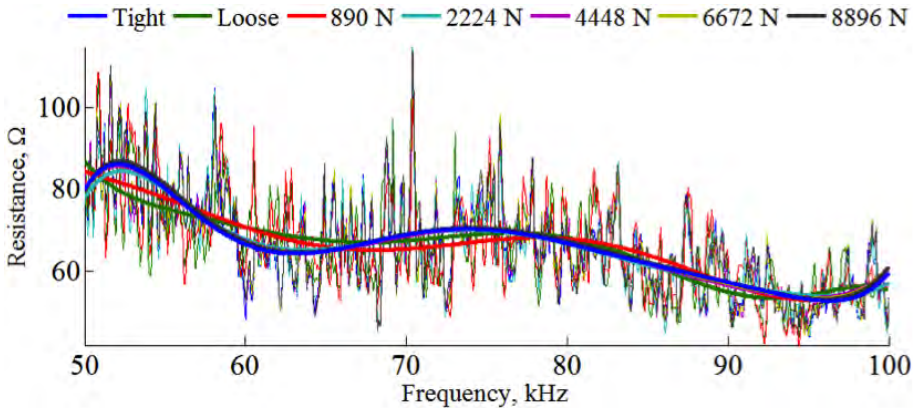

(d) Polynomial Fitting

Figure 7. Damage Detection Metrics for Bolt 5

A radically different approach to damage detection was considered in Figure 7(d). A polynomial was fit to impedance spectra corresponding to each load conditions. The polynomial-fit electro-mechanical impedance response was first introduced in 2005 for detection of cracks.[20] Figure 7(d) suggests that this approach is also successful in distinguishing loose and tight conditions of a bolted joint. Similarly to other metric, fitting of

the polynomial allows for a binary detection scenario in which first two responses (finger tight and low load) are classified as damaged and other responses classified as healthy joint. Visible in Figure 7(d), polynomial corresponding to damaged condition of the joint show different amplitude in particular frequency segments.

In summary, all presented damage metrics indicate that tests 2 (finger tight) and 3 (low load) responses varied greatly from the baseline healthy test (test 1). All subsequent tests with increased bolt load (tests 4-7) were not significantly different from the healthy test. This fact may suggest that 2224 N (500 lb_f) would be a sufficient loading for presented structural bolted joint. Applying greater loads does not impact structural integrity significantly.

4. HIGH FREQUENCY STRUCTURAL RESPONSE FROM FBG SENSORS

Structural health monitoring utilizing high frequency (hundreds of kHz) structural dynamic response has been accomplished using piezoelectric[2] and magneto-elastic[21] sensors. Our efforts have been directed towards collecting comparable high frequency dynamic signatures using fiber-optic (FBG) sensors. In order to determine if FBG sensors can provide comparable responses, multiple tests were conducted in which FBG and PZT data were collected simultaneously. The fiber-optic system allowed for acquisition of strain data in time domain. Therefore, a method of constructing the structural response from the strain data was developed.

4.1 Construction of FBG frequency response function from time-domain strain data

The FBG system synchronously measured strain data from five sensors at 500 kHz for approximately 16.7s while the piezoelectric transducer excited the structure at frequencies between 50-100kHz. In order to construct the structural response from this time-domain data the following steps were taken: (1) calculate the FFT of time domain data, (2) locate local maxima in frequency range of PZT excitation (50-100 kHz), (3) connect local maxima to build the structural response.

The process is outlined for a single test (FBG A under excitation from PZT 2) in Figure 8 . A few things needs to be kept in mind while analyzing these data. Due to PZT and FBG systems not being triggered simultaneously, the FBG system did not always see the entire frequency range. Additionally, the FBG system consistently reported a large peak at ∼75kHz which was not seen by the PZT system. It is believed that this is due to the hardware of the FBG system and is not indicative of the test specimen itself. This peak was removed before comparison to PZT system.

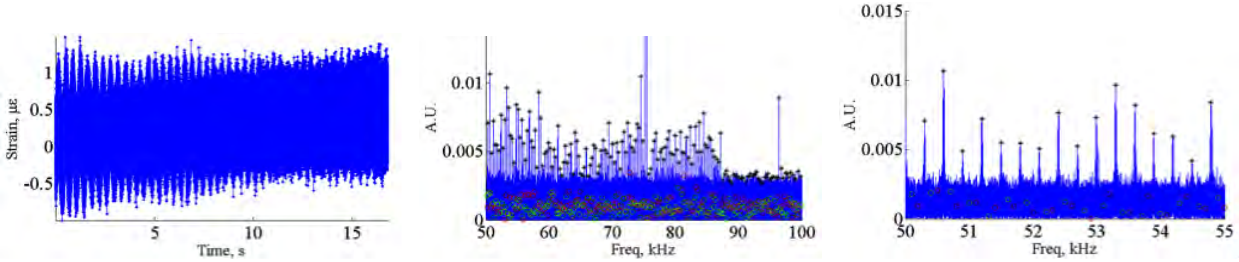

(a) Time-domain strain data (b) Peak finding routine (c) Local maxima

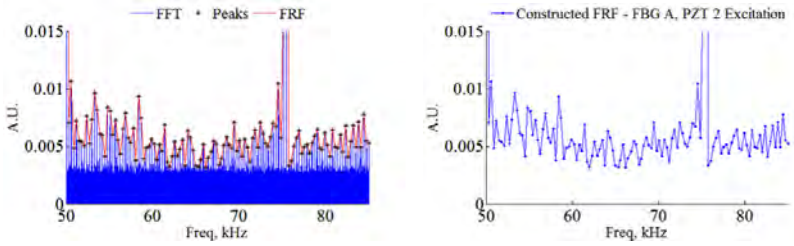

(d) Connected local maxima (e) Constructed structural response

Figure 8. Process for constructing structural response from FBG strain data

4.2 Comparison of EMI and FBG data

Structural responses constructed using a procedure outlined in previous section were compared to responses of piezoelectric sensors. From Figure 8(c) it is clear that there are local maxima in the FFT that come at regular intervals corresponding to frequency steps in the piezoelectric sensor excitation. The maximum point corresponds to structural response amplitude at that frequency. Because of this it is reasonable to compare the structural response generated by the PZT and the structural response constructed from FBG strain data. In order to validate the structural response constructed from the FBG data, the FBG structural response were plotted on the same figure with impedance responses collected by piezoelectric sensors. Examples are shown in Figure 9 for FBG A when PZT 2 was exciting the structure. Both healthy joint (T1) and loose joint (T2) conditions are presented.

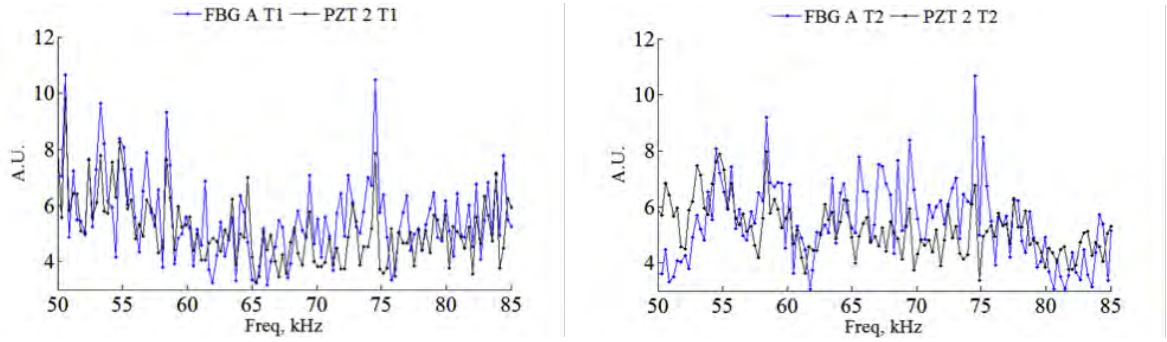

(a) Tight bolt (CC=0.652) (b) Loose bolt (CC=0.493)

Figure 9. Comparison of PZT response and FBG response for a bolted joint

In Figure 9 and subsequent figures the y-axis has been scaled arbitrarily to yield comparable magnitudes between the two systems. Visual inspection of Figure 9 suggest similar features in responses obtained using FBG and piezoelectric sensors. Many frequency peaks are aligned and relative amplitudes in particular frequency segment (e.g. 65-75 kHz in Figure 9 match). In order to quantify how close responses obtained with fiber-optic system were to the impedances collected with piezoelectric sensors, the correlation coefficients between the two responses were calculated. Correlation coefficients for cases presented in Figure 9 were found to be 0.652 and 0.493 for the tight and loose tests, respectively. This was determined to be reasonable correlation because of substantial differences between two measurement systems and the fact that the sensors were not exactly collocated. Additional difference may arise due to piezoelectric sensors measuring the structure in all directions versus the unidirectional FBG sensors.

4.3 Loose bolt detection using FBG structural response

After the capability of FBG sensors to measure high frequency responses comparable to traditional EMI methods was verified, the next goal was to determine if the FBG sensors could reliably detect damage of a bolted joint. Three separate tests were run where a different bolt was studied. Each time the closest piezoelectric sensor was used to excite the structure while all five FBG sensors simultaneously collected strain data. The first test examined bolt 3 under excitation from PZT 2. This is the data shown above in Figure 9 . The comparisons of the tight and loose responses from each system are given in Figure 10 . The second test examined bolt 5 under excitation from PZT 5 with corresponding response data given in Figure 11. The third test examined hinge 1, bolt 2 under excitation from PZT 7 with corresponding response data given in Figure 12.

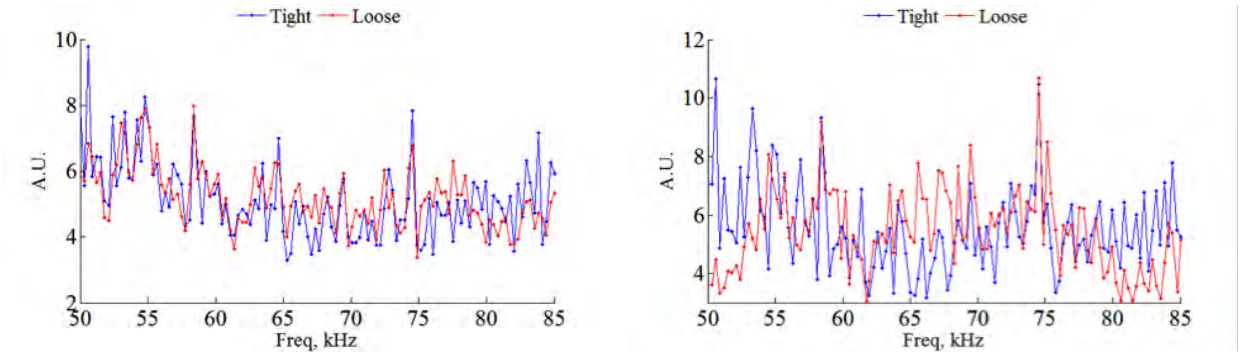

(a) PZT system tight vs. loose (b) FBG system tight vs. loose

Figure 10. Response when bolt 3 is interrogated using excitation from PZT 2

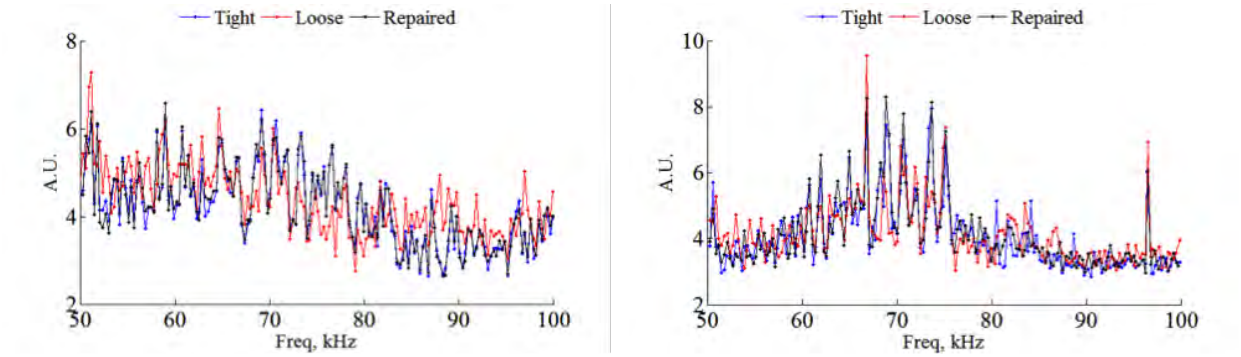

(a) PZT system tight vs. loose (b) FBG system tight vs. loose

Figure 11. Response when bolt 5 is interrogated using excitation from PZT 5

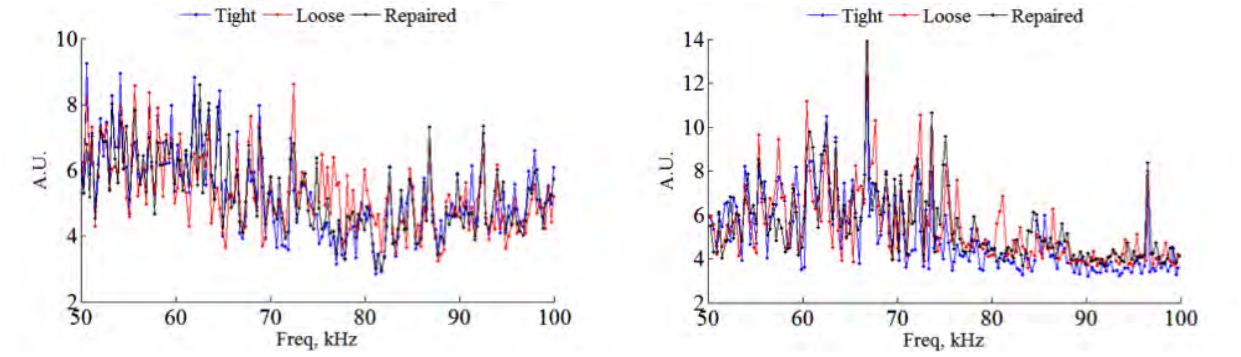

(a) PZT system tight vs. loose (b) FBG system tight vs. loose

Figure 12. Response when hinge 1, bolt 2 is interrogated using excitation from PZT 7

Damage detection metrics presented in equations (3) and (4) were explored to quantify differences between responses corresponding to healthy and damaged conditions. RMSD and CCD values are given in Table 1 for all three bolts while results obtained with the energy method and polynomial fitting are presented in Figures 13 - 15 .

Table 1. RMSD and CCD values for damage detection

Test	RMSD - PZT	RMSD - FBG	CCD - PZT	CCD - FBG
Bolt 3 Loosened	0.1703	0.3080	0.3369	0.7706
Bolt 5 Loosened	0.1679	0.1779	0.3645	0.3315
Bolt 5 Repaired	0.0373	0.1035	0.0168	0.0928
Hinge 1 Bolt 2 Loosened	0.1747	0.2438	0.3037	0.2934
Hinge 1 Bolt 2 Repaired	0.1104	0.2048	0.1156	0.2070

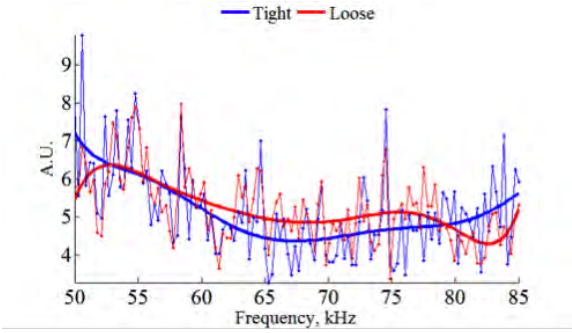

(a) Polynomial Fit of PZT Data

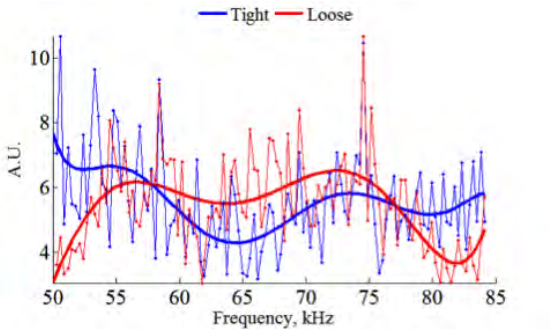

(b) Polynomial Fit of FBG Data

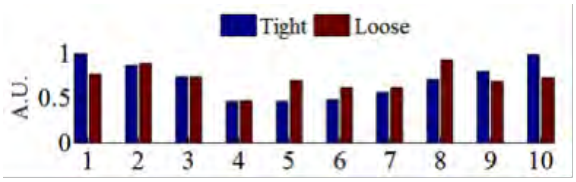

(c) Energy Distribution of PZT Data

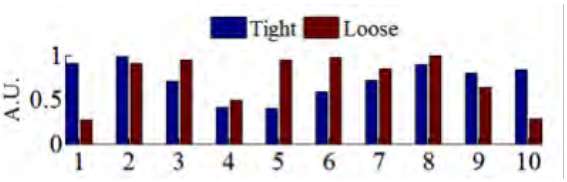

(d) Energy Distribution of FBG Data

Figure 13. Damage metrics from Bolt 3 when PZT 2 excites structure

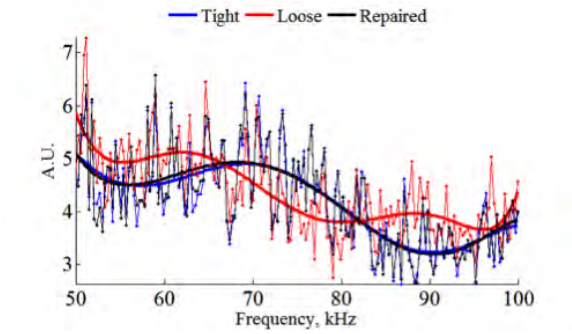

(a) Polynomial Fit of PZT Data

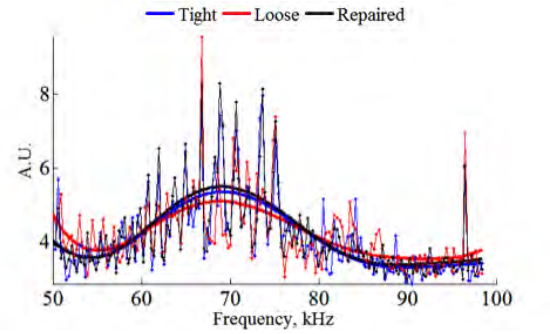

(b) Polynomial Fit of FBG Data

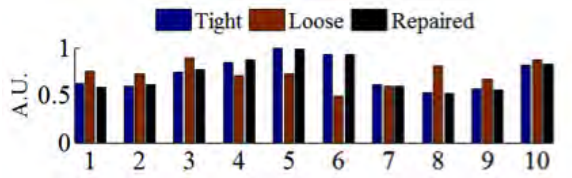

(c) Energy Distribution of PZT Data

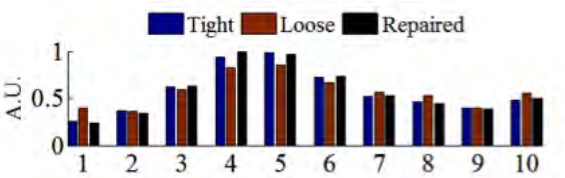

(d) Energy Distribution of FBG Data

Figure 14. Damage metrics from Bolt 5 when PZT 5 excites structure

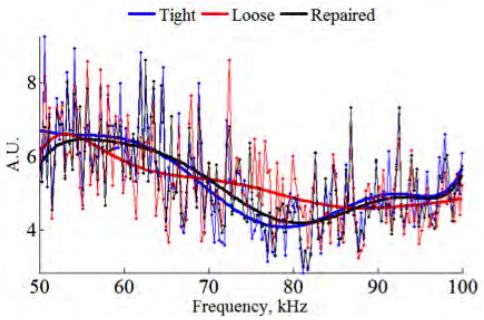

(a) Polynomial Fit of PZT Data

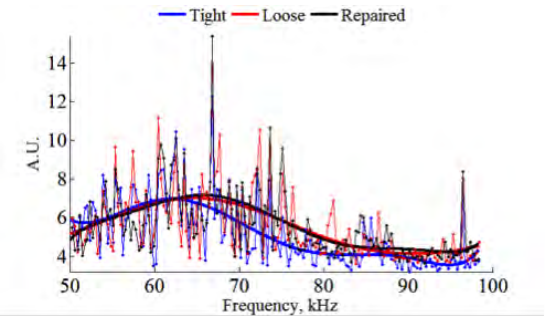

(b) Polynomial Fit of FBG Data

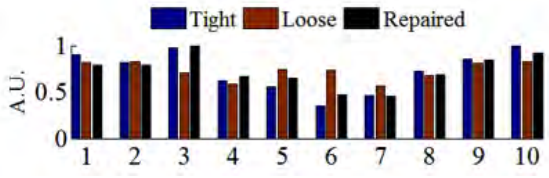

(c) Energy Distribution of PZT Data

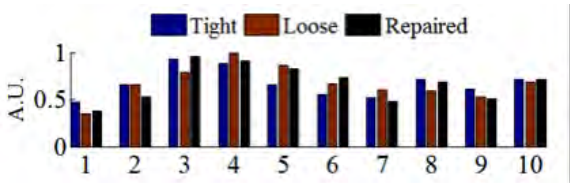

(d) Energy Distribution of FBG Data

Figure 15. Damage metrics from Hinge 1, bolt 2 when PZT 7 excites structure

Looking at the results from the fiber-optic system, we see that bolt 3 and bolt 5 could reliably be tested using both the EMI methods and the fiber-optic measurements. CCD values were determined to be the best metric for damage detection. When examining the hinge bolt, the difference between damaged and healthy cases reflected in values of the RMSD and CCD metrics are not as obvious. Examination of the polynomial fits for each test suggests that the loosened case is typically visually apparent except for the test examining the hinge bolt. This could be due to not properly tightening the hinge bolt for the repaired case.

A benefit of using the FBG system for SHM is the simultaneous data collection from all the sensors. This feature allows us to perform cross spectrum damage detection, i.e. look at data from an FBG sensor not located near the piezoelectric sensor that was exciting the structure. As an example of this approach FBG A (near bolt 3) data was analyzed when PZT 5 (near bolt 5) was exciting the structure. The resulting damage detection metrics are given in Table 2 and Figure 16. It can be seen that the fiber optic system was able to detect the damage using cross spectrum measurement

Table 2. RMSD and CCD values for cross spectrum damage detection

Test	RMSD - PZT	RMSD - FBG	CCD - PZT	CCD - FBG
Bolt 5 Loosened	0.1679	0.1806	0.3645	0.4543
Bolt 5 Repaired	0.0373	0.1423	0.0168	0.2161

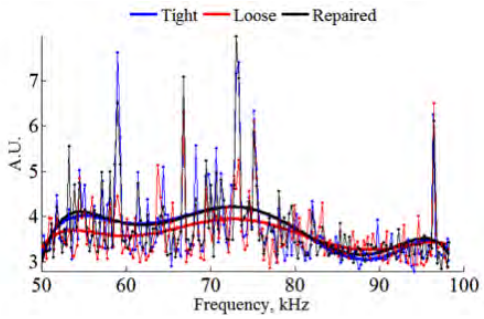

(a) Polynomial Fit of FBG Cross Spectrum Data

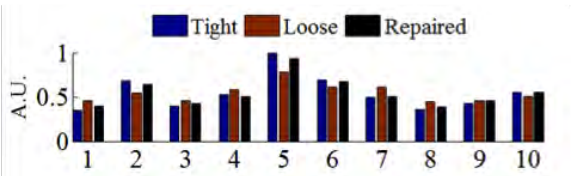

(b) Energy Distribution of FBG Cross Spectrum Data

Figure 16. Cross Spectrum Damage Metrics

5. CONCLUSION

In this contribution, we explored different electro-mechanical impedance damage detection metrics for assessing structural integrity of bolted joints and presented an alternative fiber-optic procedure for obtaining high frequency structural response analogous the electro-mechanical impedance spectra. Correlation coefficient deviation (CCD) was determined as the best metric. Alternative approaches such as polynomial fitting and energy calculation in spectral segments were also considered. Energy-based metric gives reasonable estimation of damage and in extreme cases approaches either determining area under whole impedance curve or having segments corresponding to sampling of impedance curve in which case we recover impedance spectrum. Polynomial fit metric shows good potential for detection of loose bolts but depends on the fitting procedure (polynomial order, end points, etc.).

It has been demonstrated that the fiber-optic system can collect a dynamic frequency response analogous to structural response obtained in electro-mechanical impedance method. Comparison of responses show significant similarities with high correlation coefficients between piezoelectric and fiber-optic data acquisitions. Discrepancies arise due to differences between systems (response of electronics, non-synchronous data collection, etc.), non-collocation of piezoelectric and fiber-optic sensors, and each sensor directivity. It has been shown that the high frequency structural responses collected with fiber-optic sensors can be successfully used in monitoring of structural integrity of a bolted joint using a variety of metrics. One particular advantage of the fiber-optic system is its ability to collect simultaneously responses from multiple sensors on one fiber. This approach enables structural health monitoring using cross-spectrum measurements, which is not available in a traditional electro-mechanical impedance method.

6. ACKNOWLEDGEMENTS

This work was supported by NASA Phase 1 STTR Contract No. NNX13CD08P. We thank Levy Oblea for assistance with the optical hardware.

REFERENCES

[1] Giurgiutiu, V., [*Structural Health Monitoring: with Piezoelectric Wafer Active Sensors*], Academic Press (2007).

[2] Park, G., Sohn, H., and Farrar, C., "Overview of piezoelectric impedance-based health monitoring and path forward," *Shock and Vibration Digest* (2003).

[3] Boller, C., Chang, F.-K., and Fujino, Y., eds., [*Encyclopedia of Structural Health Monitoring*], Wiley (2009).

[4] Lu, Y. and Michaels, J. E., "A methodology for structural health monitoring with diffuse ultrasonic waves in the presence of temperature variations," *Ultrasonics* **43**(9), 717–731 (2005).

[5] Yu, L., Momeni, S., Godinez, V., Giurgiutiu, V., Ziehl, P., and Yu, J., "Dual mode sensing with low-profile piezoelectric thin wafer sensors for steel bridge crack detection and diagnosis," *Advances in Civil Engineering* (2012).

[6] Black, R. J. and Moslehi, B., "Fiber bragg grating interrogators for structural health monitoring." presented at the Soc. Adv. Mater. Process. Eng. (2008).

[7] Hill, K. O., Fujii, Y., Johnson, D. C., and Kawasaki, B. S., "Photosensitivity in optical fiber waveguides: Application to reflection filter fabrication," *Applied Physics Letters* (2008).

[8] Werneck, M. M., Allil, R. C. S. B., Ribeiro, B. A., and de Nazare, F. V., [*Current Trends in Short- and Long-period Fiber Gratings*], ch. A Guide to Fiber Bragg Grating Sensors, InTech (2013).

[9] Sun, F., Chaudhry, Z., Liang, C., and Rogers, C., "Truss structure integrity identification using pzt sensor–actuator," *Journal of Intelligent Material Systems and Structures* **134-139** (1995).

[10] Liang, C., Sun, F., and Rogers, C., "Coupled electro-mechanical analysis of adaptive material systems-determination of the actuator power consumption and system energy transfer," *Journal of Intelligent Material Systems and Structures* **5** (1994).

[11] Liang, C., Sun, F. P., and Rogers, C. A., "An impedance method for dynamic analysis of active material systems," in [*34th AIAA/ASME/ASCE/AHS/ASC SDM Conference*], (1993).

[12] Chaudhry, Z., Lalande, F., Ganino, A., Rogers, C. A., and Chung, J., "Monitoring the integrity of composite patch structural repair via piezoelectric actuators/sensors," in [*36th AIAA/ASME/ASCE/AHS/ASC SDM Conference*], (1995).

[13] Giurgiutiu, V. and Rogers, C. A., "Experimental investigation of e/m impedance health monitoring for spot-welded structural joints," *Journal of Intelligent Material Systems and Structures* (1997).

[14] Park, G., Kabeya, K., Cudney, H., and Inman, D., "Impedance-based structural health monitoring for temperature varying applications," *JSME International Journal* **42**(2), 249–258 (1999).

[15] Zagrai, A. and Giurgiutiu, V., "Electro-mechanical impedance method for crack detection in thin plates," *Journal of Intelligent Material Systems and Structures* (2001).

[16] Tseng, K.-H. and Naidu, A., "Non-parametric damage detection and characterization using smart piezoceramic material," *Smart Materials and Structures* **11**, 317–329 (2002).

[17] Bhalla, S. and Soh, C., "Electromechanical impedance modeling for adhesively bonded piezo-transducers," *Journal of Intelligent Material Systems and Structures* **15**, 955–972 (2004).

[18] Mascarenas, D., Todd, M., Park, G., and Farrar, C., "A miniaturized electromechanical impedance-based node for the wireless interrogation of structural health," in [*SPIE on Health Monitoring and Smart Nondestructive Evaluation of Structural and Biological Systems V*], (2006).

[19] Giurgiutiu, V., Zagrai, A., and Bao, J. J., "Piezoelectric wafer embedded active sensors for aging aircraft structural health monitoring," *International Journal of Structural Health Monitoring* **1** (2002).

[20] Giurgiutiu, V. and Zagrai, A., "Damage detection in thin plates and aerospace structures with the electromechanical impedance method," *International Journal of Structural Health Monitoring* **4**(2), 99–118 (2005).

[21] Conrad, D. and Zagrai, A., "Active detection of structural damage in aluminum alloy using magneto-elastic active sensors (meas)," in [*SMASIS-11, ASME Conference on Smart Materials, Adaptive Structures*], (2011).